Matter and Radiation at Extremes | RESEARCH ARTICLE | scitation.org/journal/mre

Observation of Zeeman splitting effect in a laser-driven coil

Cite as: Matter Radiat. Extremes 7, 024402 (2022); doi: 10.1063/5.0060954
Submitted: 23 June 2021 • Accepted: 16 January 2022 •
Published Online: 16 February 2022

Baojun Zhu,[1,2,a] Zhe Zhang,[1,3,b] Chang Liu,[4] Dawei Yuan,[5] Weiman Jiang,[1] Huigang Wei,[5] Fang Li,[1] Yihang Zhang,[1] Bo Han,[6] Lei Cheng,[1] Shangqing Li,[1] Jiayong Zhong,[6] Xiaoxia Yuan,[7] Bowei Tong,[6] Wei Sun,[6] Zhiheng Fang,[8] Chen Wang,[8] Zhiyong Xie,[8] Neng Hua,[9] Rong Wu,[9] Zhanfeng Qiao,[9] Guiyun Liang,[5] Baoqiang Zhu,[9] Jianqiang Zhu,[9] Shinsuke Fujioka,[2] and Yutong Li[1,3,10]

AFFILIATIONS

[1]Beijing National Laboratory of Condensed Matter Physics, Institute of Physics, CAS, Beijing 100190, China
[2]Institute of Laser Engineering, Osaka University, 2-6 Yamada-oka, Suita, Osaka, Japan
[3]Songshan Lake Materials Laboratory, Dongguan, Guangdong 523808, China
[4]Department of Advanced Photon Research, Kansai Photon Science Institute, National Institutes for Quantum and Radiological Science and Technology, 619-0215 Kyoto, Japan
[5]Key Laboratory of Optical Astronomy, National Astronomical Observatories, Chinese Academy of Sciences, Beijing 100101, China
[6]Department of Astronomy, Beijing Normal University, Beijing 100875, China
[7]Center for Advanced Material Diagnostic Technology, College of Engineering Physics, Shenzhen Technology University, Shenzhen 518118, China
[8]Shanghai Institute of Laser Plasma, Shanghai 201800, China
[9]National Laboratory on High Power Laser and Physics, Shanghai Institute of Optics and Fine Mechanics, Chinese Academy of Sciences, Shanghai 201800, China
[10]School of Physical Sciences, University of Chinese Academy of Sciences, Beijing 100049, China

Note: This paper is part of the Special Issue on Magnetized Plasmas in HED.
[a]**Author to whom correspondence should be addressed:** baojunzhu@ile.osaka-u.ac.jp
[b]**Electronic mail:** zzhang@iphy.ac.cn

ABSTRACT

The Zeeman splitting effect is observed in a strong magnetic field generated by a laser-driven coil. The expanding plasma from the coil wire surface is concentrated at the coil center and interacts with the simultaneously generated magnetic field. The Cu I spectral lines at wavelengths of 510.5541, 515.3235, and 521.8202 nm are detected and analyzed. The splittings of spectral lines are used to estimate the magnetic field strength at the coil center as ~31.4 ± 15.7 T at a laser intensity of ~5.6×10^{15} W/cm^2, which agrees well with measurements using a B-dot probe. Some other plasma parameters of the central plasma disk are also studied. The temperature is evaluated from the Cu I spectral line intensity ratio, while the electron density is estimated from the Stark broadening effect.

I. INTRODUCTION

The Zeeman effect was one of the most significant spectroscopic discoveries of the nineteenth century. It has been applied in various research fields since it was observed in 1896.[1] In atomic and molecular physics, the Zeeman effect plays a key role in calculating hyperfine atomic structures.[2] In materials science, for example, the observed Zeeman splitting and oscillator strengths reveal the symmetry and fine crystal structure of Cr-doped GaAs.[3] In fusion research, the Zeeman effect is used not only to measure the magnetic field (B-field) strength, but also to study impurities in particle transport in magnetically confined fusion plasmas through determination of line positions, shapes, and hence species temperatures.[4,5] In astrophysics, the Zeeman effect makes it possible to infer the B-field strength in

various remote objects from telescope observations.[6–9] This is of great help in understanding the evolution of these objects and related astrophysical phenomena, such as jets[10] and magnetic reconnection.[11,12] In laser–plasma research, the Zeeman effect is a powerful tool for measuring the intensity of strong B-fields at local plasma positions.[13,14] It is very helpful in studies of strongly magnetized plasmas, in the context, for example, of magnetized fast ignition[15] and magnetohydrodynamic effects.[16]

In recent years, laser-driven coils have shown promise for laboratory generation of B-fields.[17–25] This method of B-field generation has attracted interest in many areas of research owing to the high field amplitudes that it can achieve and its controllable characteristics. A variety of techniques have been used to measure a rapidly rising B-field with small spatial and short temporal scales. One traditional method is to use a differential magnetic probe, also known as a B-dot probe.[17,19,20] This probe provides information on both the amplitude and temporal evolution of a B-field. However, it is vulnerable to the electromagnetic noise generated by laser–plasma interactions and cannot measure local B-fields directly. It can only be deployed several centimeters away from the coil center, and consequently the values of smaller B-fields (of the order of 10^2–10^3 T) at the coil center have to be extrapolated from measured B-fields of only 10^{-4}–10^{-1} T. Another new approach to the measurement of laser-generated B-fields is through Faraday rotation,[18,20,24] which can also provide both the amplitude and temporal evolution of the B-fields. However, this technique usually requires an external synchronized polarized light probe and a magneto-optical crystal positioned several millimeters away from the coil center. The main limitation of this diagnostic is the opacity of magneto-optical crystals and the consequent blacking out of light signals.[18] Another diagnostic for laser-driven B-fields is provided by proton radiography.[20–22,26] This measurement method can infer the local B-field distribution, but an additional relativistic laser is needed to generate high-energy protons. The temporal range is usually about 100 ps.

In this study, the Zeeman effect is applied for the first time to measure the B-field generated by a laser-driven coil. The copper plasma expanding from the coil surface to the coil center is used as an emission source. We choose the Cu I $3d^{10}4p^2P^0_{3/2} \rightarrow 3d^9 4s^{22}D_{5/2}$, $3d^{10}4d^2D_{3/2} \rightarrow 3d^{10}4p^2P^0_{1/2}$, and $3d^{10}4d^2D_{5/2} \rightarrow 3d^{10}4p^2P^0_{3/2}$ spectral lines emitted from the hot plasma. Their wavelengths are 510.5541, 515.3235, and 521.8202 nm, respectively.

II. EXPERIMENTS

The experiments were performed at the Shengguang-II laser facility. An Ω-shaped copper coil was employed, with the configuration is shown in Fig. 1(b). The inner diameter of the coil was 0.8 mm, and its opening width was 0.5 mm. The coil wire had a cross section of 200 × 200 μm^2. The diameter of the disk end was ~1 mm. The coil axis was parallel to the z axis. The experimental setup is illustrated in Fig. 1(a). Eight laser beams with a total energy of ~2 kJ were divided into two bunches and focused onto two sides of the bottom disk of the Ω-shaped coil target at a wavelength of 351 nm and duration of 1 ns. The focal spot was about 150 μm in full width at half maximum (FWHM). The laser intensity was ~5.6 × 10^{15} W/cm^2. A strong magnetic field was generated at the coil center due to the cold-electron return current from the focal spot to the top end of the coil. The mechanism is the same as that in our previous studies.[19,24–26]

The coil surface was ionized as a result of simultaneous Joule heating and x-ray radiation from the laser focal spot. The surface plasma expanded toward the coil center. Shadowgraphy with a magnification of ~4 was used to detect the plasma evolution inside the coil along the $-z$ direction with a synchronized 70 ps probe laser at a wavelength of 527 nm. The Zeeman effect was used to detect the laser-driven B-field strength. The central hot plasma was used as an emission source, and this was imaged onto a spectrometer entrance slit 20 μm wide with a total magnification of ~1.7. The image was transformed into spectral signals on an intensified charged coupled device (ICCD) after diffraction by a grating with 150 grooves/mm. The spectral resolution was ~0.39 nm. The axis of the first collection lens was at ~15° to the axis of the Ω-shaped coil. In addition, a differential B-dot probe was also used to measure the B-field strength for comparison. It was placed ~3 cm away from the coil center, with the pickup coil plane in the x–y plane at z = 0.

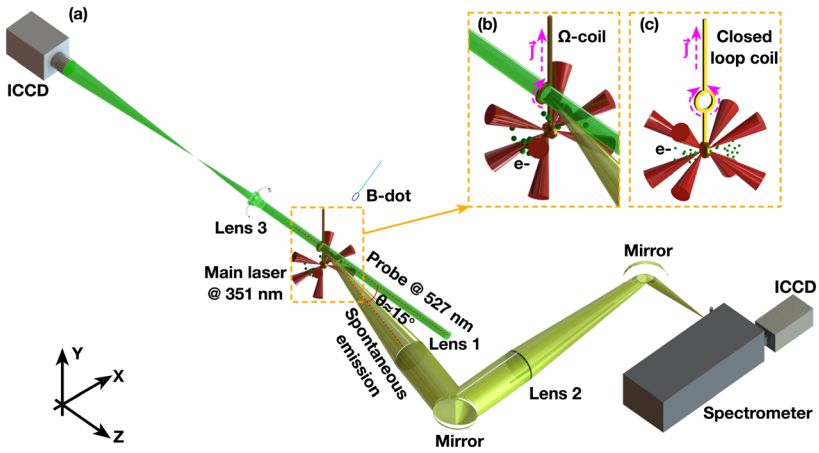

FIG. 1. (a) Experimental setup. (b) Configuration of Ω-shaped coil. (c) Configuration of closed-loop coil.

III. RESULTS AND DISCUSSION

A. Magnetic fields measured with B-dot probe

Figure 2 shows the temporal evolution of the average B_z (the z component of the B-field strength) at the B-dot probe position at a laser intensity of ~5.6 × 10^{15} W/cm^2. The peak magnetic field measured at the local B-dot position, $B_{\text{B-dot}}$, was 0.020 ± 0.002 T. The spatial distribution of the magnetic field was calculated using the three-dimensional magnetostatic code RADIA.[27] The whole target geometry, including the open coil and the straight wires, was modeled precisely to allow accurate extrapolation of the magnetic field distribution. The current in the coil was adjusted to match the calculated field strength with the measured value at the position of the B-dot probe. The peak current in the coil target was estimated to be ~38 kA. Figure 3(a) shows the calculated two-dimensional magnetic field distribution in the x–y plane at z = 0 with the peak current. The B-field strength at the coil center, B_{center}, was estimated to be 22.9 ± 0.1 T.

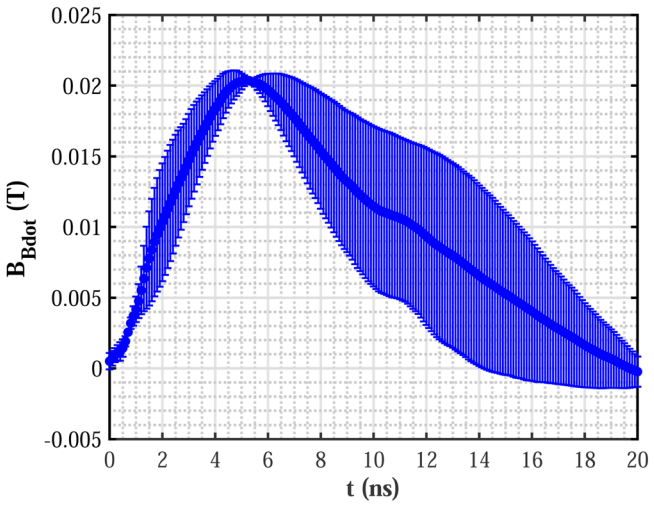

FIG. 2. Temporal evolution of the measured B-field strength at the position of the B-dot probe. The vertical error bars correspond to the standard deviation of two shots.

B. Zeeman measurements

Figure 4 shows temporally resolved shadowgraphs before and after a laser shot. Compared with the shadowgraph before the laser shot in Fig. 4(a), Fig. 4(b) at a delay time of 3.5 ns shows an obvious increase in wire width. This demonstrates that the coil surface is ionized. This is probably due to Ohmic heating and x-ray radiation. The ionized plasma has expanded from the coil's inner surface toward its center. Figure 4(c) at 6.0 ns reveals a higher plasma concentration that has formed a high-density area at the coil center. This central plasma with a width of ~395 μm along the y axis was employed as an emission source in our experiments using the Zeeman effect to detect the local B-field strength at the coil center.

In our Zeeman measurements, three Cu I transitions were selected: (1) $3d^{10}4p^2P^0_{3/2} \rightarrow 3d^9 4s^{22}D_{5/2}$, (2) $3d^{10}4d^2D_{3/2} \rightarrow 3d^{10}4p^2P^0_{1/2}$, and (3) $3d^{10}4d^2D_{5/2} \rightarrow 3d^{10}4p^2P^0_{3/2}$. According to the theory of the Zeeman effect,[1,28] two σ components should be detected, because the observation angle is nearly parallel to the magnetic field. By comparing the time-integrated spectrum of the Ω-shaped coil and that obtained from the NIST Atomic Spectra Database[29] shown in Fig. 5(a), the Cu I lines at these three transitions exhibit an obvious splitting. The experimental π component was deduced from the center of neighboring pairs of σ peaks. The respective wavelengths were 510.42, 515.16, and 521.47 nm. The splitting distance $\Delta\lambda_B$ between the σ and π lines was 0.39 nm for all three transitions. In addition, compared with the NIST spectrum,[29] the π line shifted owing to Doppler effects. These results demonstrate that the central plasma propagated in the z direction. The velocity was estimated to be ~129.6 ± 39.8 km/s.

To verify the role of B-fields, a closed copper loop target was also used in our experiments. The structure of this coil is shown in Fig. 1(c). The inner diameter and cross section of the coil, as well as the experimental setup, were the same as those used for the Ω-shaped coil. The only difference was that the coil was a closed loop, rather than an open configuration. Compared with the Ω-shaped coil, the return current flowed symmetrically along the closed loop. Therefore, the B-field strength at the coil center was, in theory, zero, as shown in Fig. 3(b). The red line in Fig. 5(a) represents the spontaneous emission spectrum of the closed-loop coil. It is obvious that the closed-loop coil did not cause a splitting effect. Therefore, the splitting can be attributed to a B-field effect.

To evaluate the magnetic field strength for linear Zeeman effects, anomalous Zeeman effects and Paschen–Back effects[30] should first be distinguished when the spin angular momentum S is nonzero. The

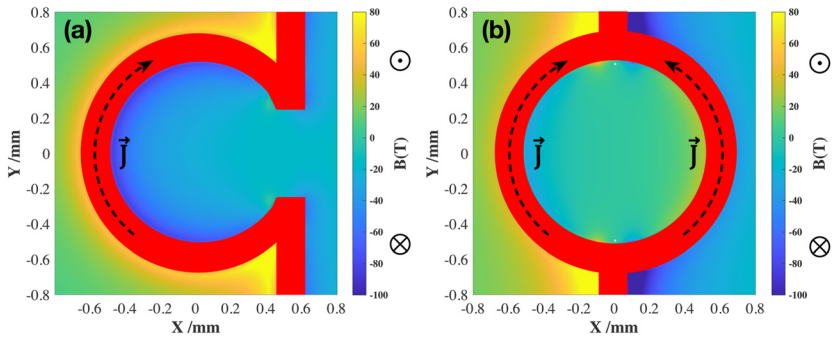

FIG. 3. Calculated two-dimensional magnetic field distribution in the x–y plane at z = 0: (a) Ω-shaped coil; (b) closed-loop coil.

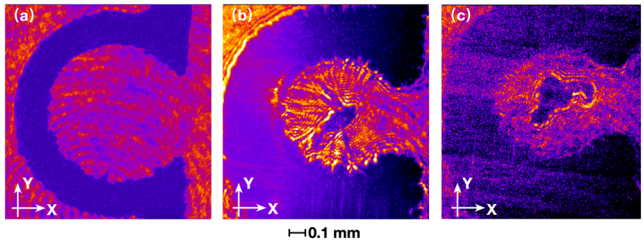

FIG. 4. Shadowgraphs in the x–y plane: (a) before laser shot; (b) at a delay time $t = 3.5$ ns; (c) at a delay time $t = 6.0$ ns. The dark regions demonstrate that the plasma density is so high that the probe light cannot penetrate it.

fine-structure split distance $\Delta\lambda_{LS}$ between transition (3) and the transition $3d^{10}4d^2D_{3/2} \rightarrow 3d^{10}4p^2P^0_{3/2}$ due to spin–orbit coupling is 0.1868 nm. Because $\Delta\lambda_{LS} < \Delta\lambda_B = 0.39$ nm, this demonstrates that the magnetic field strength was strong enough to disrupt the spin–orbit coupling, leading to spin angular momentum S and orbital angular momentum L coupling more strongly to the external magnetic field than to each other, i.e., the Paschen–Back effect. Thus, the Paschen–Back effect was dominant in our experiments. The energy shift ΔE in an external magnetic field is

$$\Delta E = \frac{ehB_{\text{center}}}{4\pi m_e}(\Delta m_l + \Delta m_s), \tag{1}$$

$$\frac{hc}{\lambda^2}\Delta\lambda = \frac{ehB_{\text{center}}}{4\pi m_e}(\Delta m_l + \Delta m_s), \tag{2}$$

where m_l and m_s are the orbital and spin magnetic quantum numbers, respectively, h is Planck's constant, e and m_e are the electron charge and mass, respectively, and λ is the detection wavelength. The average B_{center} was calculated to be ~31.4 T according to Eq. (2). The details of the Zeeman measurements are summarized in Table I. Considering the low spectral resolution in our experiments, the splitting error bar was

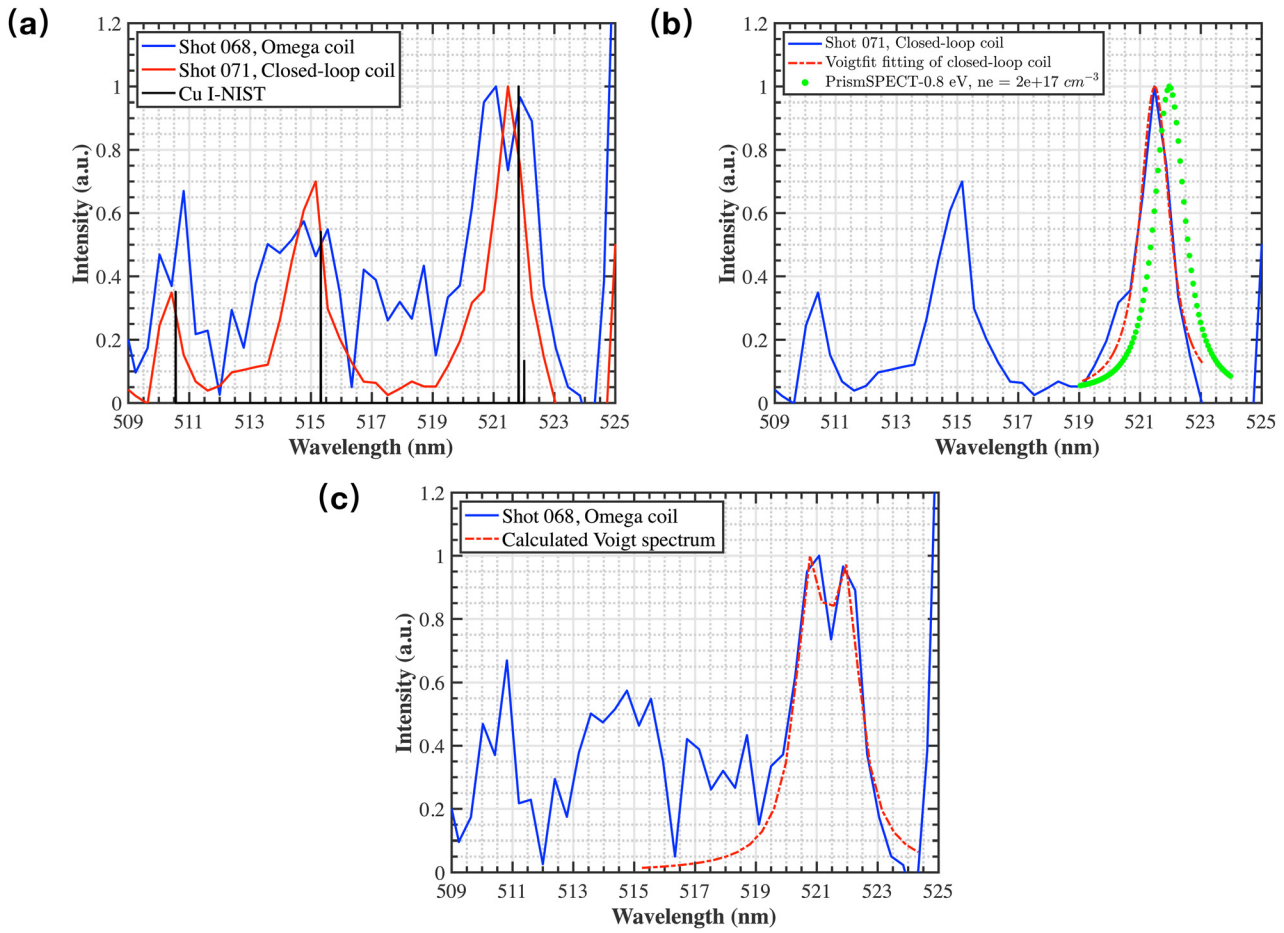

FIG. 5. (a) Comparison between the observed spectra from the Ω-shaped and closed-loop coils and the Cu I spectrum obtained from the NIST Atomic Spectra Database at $T_e = 0.8$ eV. (b) Comparison between the observed spectrum from the closed-loop coil and calculated spectra: the red dashed curve is the Voigt fitting for the closed-loop coil spectrum at 521.47 nm, and the green dotted curve is one typical PrismSPECT Cu I line shape convolved with instrumental broadening computed at $T_e = 0.8$ eV and $n_e = 2 \times 10^{17}$ cm^{-3}. (c) Comparison between the observed spectrum from the Ω-shaped coil and the calculated Voigt spectrum.

TABLE I. Summary of spectra.

Theoretical wavelength (nm)	510.5541	515.3235	521.8202
Experimental π wavelength (nm)	510.42	515.16	521.47
Transition	$3d^{10}4p^2P^0_{3/2}$ ↓ $3d^9 4s^{22}D_{5/2}$	$3d^{10}4d^2D_{3/2}$ ↓ $3d^{10}4p^2P^0_{1/2}$	$3d^{10}4d^2D_{5/2}$ ↓ $3d^{10}4p^2P^0_{3/2}$
Upper energy level E (eV)	3.82	6.19	6.19
A (s^{-1})	2.0×10^6	6.0×10^7	7.5×10^7
g_k	4	4	6
Doppler shift (nm)	0.1341	0.1635	0.3502
Velocity (km/s)	81.6	98.6	208.6
Average velocity (km/s)		129.6 ± 39.8	
Splitting $\Delta\lambda_B$ between σ and π (nm)	0.39	0.39	0.39
B_{center} (T)	32.0 ± 16.0	31.4 ± 15.7	30.7 ± 15.4
Average B_{center} (T)		31.4 ± 15.7	

estimated to be the spectral resolution. Therefore, the splitting distance between the two σ lines was 0.39–1.18 nm, and the average B_{center} was 31.4 ± 15.7 T. This value is consistent with the value measured with the B-dot probe.

One advantage of measuring the Zeeman effect compared with other B-field measurements is that the electron temperature T_e and density n_e can be derived from the line shapes and relative intensities of some atomic lines. In our experiments, the line intensity ratio between transitions (1) and (3), I_1/I_3, was used to calculate the plasma temperature T_e. According to the Boltzmann equation, under the assumption of local thermodynamic equilibrium (LTE),

$$\frac{I_1}{I_3} = \frac{g_1 A_1}{g_3 A_3}\frac{\lambda_3}{\lambda_1}\exp\left(-\frac{E_1 - E_3}{T_e}\right), \tag{3}$$

where g is the statistical weight, A is the Einstein transition probability of spontaneous emission, E is the upper energy level, and λ is the corresponding wavelength. All of these parameters shown in Table I were obtained from the NIST Atomic Spectra Database.[29] The ratio I_1/I_3 was calculated to be 0.57 ± 0.04 for the Ω-shaped coil and 0.71 for the closed-loop coil. The error bar corresponded to the intensity difference at the separated peaks. T_e was then estimated to be 0.73 ± 0.04 and 0.80 eV for the Ω-shaped and closed-loop coils, respectively, and thus was almost the same for both coil configurations.

The spectral width at transition (3) of the closed-loop target was used to derive the electron density n_e. The spectral shape of the Cu I multiplet was mainly affected by Stark broadening, Doppler broadening, and instrumental broadening. Because Stark broadening has a Lorentz profile, while Doppler and instrumental broadening have Gaussian profiles, the whole spectral profile should be a convolution of Gaussian (G) and Lorentzian (L) profiles. Therefore, to obtain accurate FWHM values, the Voigt function was applied to fit the experimental spectra shape. The Voigt function is expressed as

$$V = \int_{-\infty}^{+\infty} G(\lambda', \omega_G) L(\lambda - \lambda', \omega_L)\, d\lambda, \tag{4}$$

with

$$\omega_G = \sqrt{\omega_d^2 + \omega_i^2}, \tag{5}$$

$$\omega_L = \omega_s, \tag{6}$$

where λ is the wavelength, ω is the FWHM for each profile, and ω_s, ω_d, and ω_i are the FWHM values of the Stark, Doppler, and instrumental broadenings, respectively. According to the experimental conditions, ω_i was 0.39 nm. Taking the sound speed to be approximately equal to the plasma expansion velocity, we obtain $ZT_e + \gamma T_i = 111.2 \pm 68.3$ eV,[31] where γ is the adiabatic index. Therefore, T_i is less than 200 eV. The maximum Doppler broadening is of the order of 10^{-2} nm, which can be neglected compared with ω_i. ω_G is mainly determined by ω_i. Then, the total FWHM ω_{ex} at transition (3) could be derived from the Voigt fitting curve shown in Fig. 5(b) with a fixed calculated ω_G. ω_{ex} was calculated to be 1.16 ± 0.18 nm, while ω_s was 1.02 ± 0.21 nm. The dependence of the total FWHM ω_V on n_e was calculated using the collisional–radiative simulation software PrismSPECT.[32] In our simulations, all of the broadening mechanisms mentioned above were included. The simulations were performed under LTE conditions.

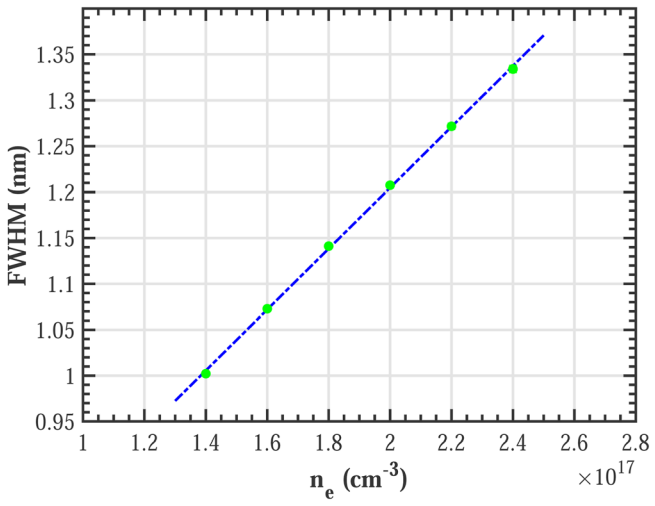

FIG. 6. FWHM of line at transition (3) as a function of electron density n_e computed with PrismSPECT at T_e = 0.8 eV.

The total FWHM ω_V of line transition (3) calculated by PrismSPECT, presented in Fig. 6, shows a linear dependence on the electron density n_e. According to the FWHM found experimentally, the electron density was $(1.86 \pm 0.55) \times 10^{17}$ cm^{-3}. A similar calculation was also performed at transition (2), where n_e was estimated to be $(2.28 \pm 0.35) \times 10^{17}$ cm^{-3}. This value agrees well with that at transition (3). The average electron density was $(2.07 \pm 0.33) \times 10^{17}$ cm^{-3}. In addition, we also calculated the Voigt broadening profile for the Ω-shaped coil at transition (3). We also accounted for ω_s, ω_d, and ω_i estimated from the closed-loop target. The calculated spectra shown in Fig. 5(c) agree well with the experimental spectrum.

IV. CONCLUSIONS

For what we believe to be the first time, the Zeeman effect has been applied to measure the local magnetic field generated by a laser-driven coil. The results show good agreement with B-dot probe measurements. Compared with other common magnetic field diagnostics, much more local plasma information, including plasma temperature and density, can be derived from the Zeeman spectra. In addition, when the magnetic field is strong enough to split ultraviolet or x-ray light, the Zeeman effect will be a very powerful diagnostic tool to detect the magnetic field inside a high-density plasma. Moreover, the rapid development of laser-driven magnetic fields also offers a new opportunity to study nonlinear Zeeman effects in the laboratory. This will open a new approach for studying astrophysical phenomena[33,34] and fundamental physics in the future.

ACKNOWLEDGMENTS

This work was supported in part by the Strategic Priority Research Program of the Chinese Academy of Sciences (Grant Nos. XDA25010100, XDA25010300, and XDA25030100), the National Natural Science Foundation of China (Grant Nos. U1930107 and 11827807), and the Japanese Ministry of Education, Science, Sports, and Culture through Grants-in-Aid, KAKENHI (Grant No. 21H04454).

AUTHOR DECLARATIONS

Conflict of Interest

The authors declare no conflicts of interest.

DATA AVAILABILITY

All data needed to evaluate the conclusions in the paper are present in the paper. Experimental data and simulations are available from the corresponding author upon reasonable request.

REFERENCES

[1]P. Zeeman, "XXXII. On the influence of magnetism on the nature of the light emitted by a sub-stance," London, Edinburgh Dublin Philos. Mag. J. Sci. **43**(262), 226–239 (1897).

[2]W. L. Virgo, "Simultaneous Stark and Zeeman effects in atoms with hyperfine structure," Am. J. Phys. **81**, 936–942 (2013).

[3]C. Uihlein and L. Eaves, "High-magnetic-field Zeeman spectroscopy of the 0.84-eV Cr-related emission and absorption line in GaAs(Cr): Experiment and theory," Phys. Rev. B **26**, 4473–4484 (1982).

[4]K. Mizushiri, K. Fujii, T. Shikama, A. Iwamae, M. Goto, S. Morita, and M. Hasuo, "A simultaneous measurement of polarization-resolved spectra of neutral helium 23P–33D, 21P–31D and 23P–33S emissions from the periphery of a Large Helical Device plasma," Plasma Phys. Controlled Fusion **53**, 105012–105024 (2011).

[5]J. D. Hey, C. C. Chu, S. Brezinsek, P. Mertens, and B. Unterberg, "Oxygen ion impurity in the TEXTOR tokamak boundary plasma observed and analysed by Zeeman spectroscopy," J. Phys. B: At., Mol. Opt. Phys. **35**, 1525–1553 (2002).

[6]D. Deming, R. J. Boyle, D. E. Jennings, and G. Wiedemann, "Solar magnetic field studies using the 12 micron emission lines. I. Quiet-sun time series and sunspot slices: Erratum," Astrophys. J. **338**, 1193 (1989).

[7]H. W. Babcock, "Zeeman effect in stellar spectra," Astrophys. J. **105**, 105 (1947).

[8]R. I. Anderson, A. Reiners, and S. K. Solanki, "On detectability of Zeeman broadening in optical spectra of F- and G-dwarfs," Astron. Astrophys. **522**, A81 (2010).

[9]J. D. Bailey, "Measuring the surface magnetic fields of magnetic stars with unresolved Zeeman splitting," Astron. Astrophys. **568**, A38 (2014).

[10]J. Ferreira, "Magnetically-driven jets from Keplerian accretion discs," Astron. Astrophys. **319**, 340–359 (1997).

[11]R. A. Kopp and G. W. Pneuman, "Magnetic reconnection in the corona and the loop prominence phenomenon," Sol. Phys. **50**, 85–98 (1976).

[12]S. Masuda, T. Kosugi, H. Hara, S. Tsuneta, and Y. Ogawara, "A loop-top hard X-ray source in a compact solar flare as evidence for magnetic reconnection," Nature **371**, 495–497 (1994).

[13]E. A. McLean, J. A. Stamper, C. K. Manka, H. R. Griem, D. W. Droemer, and B. H. Ripin, "Observation of magnetic fields in laser-produced plasma using the Zeeman effect," Phys. Fluids **27**, 1327–1335 (1984).

[14]J. Briand, J. C. Kieffer, A. Gomes, C. Arnas, J. P. Dinguirard, Y. Quemener, L. Berge, M. El Tamer, and M. Armengaud, "Measurements of magnetic fields using the Zeeman effect in laser-produced plasmas," Phys. Fluids **30**, 2893–2897 (1987).

[15]S. Sakata, S. Lee, H. Morita, T. Johzaki, H. Sawada, Y. Iwasa, K. Matsuo, K. F. F. Law, A. Yao, M. Hata, A. Sunahara, S. Kojima, Y. Abe, H. Kishimoto, A. Syuhada, T. Shiroto, A. Morace, A. Yogo, N. Iwata, M. Nakai, H. Sakagami, T. Ozaki, K. Yamanoi, T. Norimatsu, Y. Nakata, S. Tokita, N. Miyanaga, J. Kawanaka, H. Shiraga, K. Mima, H. Nishimura, M. Bailly-Grandvaux, J. J. Santos, H. Nagatomo, H. Azechi, R. Kodama, Y. Arikawa, Y. Sentoku, and S. Fujioka, "Magnetized fast isochoric laser heating for efficient creation of ultra-high-energy-density states," Nat. Commun. **9**, 3937 (2018).

[16]K. Matsuo, T. Sano, H. Nagatomo, T. Somekawa, K. F. F. Law, H. Morita, Y. Arikawa, and S. Fujioka, "Enhancement of ablative Rayleigh-Taylor instability growth by thermal conduction suppression in a magnetic field," Phys. Rev. Lett. **127**, 165001 (2021); arXiv:2106.03293.

[17]H. Daido, F. Miki, K. Mima, M. Fujita, K. Sawai, H. Fujita, Y. Kitagawa, S. Nakai, and C. Yamanaka, "Generation of a strong magnetic field by an intense CO_2 laser pulse," Phys. Rev. Lett. **56**, 846–849 (1986).

[18]S. Fujioka, Z. Zhang, K. Ishihara, K. Shigemori, Y. Hironaka, T. Johzaki, A. Sunahara, N. Yamamoto, H. Nakashima, T. Watanabe, H. Shiraga, H. Nishimura, and H. Azechi, "Kilotesla magnetic field due to a capacitor-coil target driven by high power laser," Sci. Rep. **3**, 1170 (2013).

[19]B. J. Zhu, Y. T. Li, D. W. Yuan, Y. F. Li, F. Li, G. Q. Liao, J. R. Zhao, J. Y. Zhong, F. B. Xue, S. K. He, W. W. Wang, F. Lu, F. Q. Zhang, L. Yang, K. N. Zhou, N. Xie, W. Hong, H. G. Wei, K. Zhang, B. Han, X. X. Pei, C. Liu, Z. Zhang, W. M. Wang, J. Q. Zhu, Y. Q. Gu, Z. Q. Zhao, B. H. Zhang, G. Zhao, and J. Zhang, "Strong magnetic fields generated with a simple open-ended coil irradiated by high power laser pulses," Appl. Phys. Lett. **107**, 261903 (2015).

[20]J. J. Santos, M. Bailly-Grandvaux, L. Giuffrida, P. Forestier-Colleoni, S. Fujioka, Z. Zhang, P. Korneev, R. Bouillaud, S. Dorard, D. Batani, M. Chevrot, J. E. Cross, R. Crowston, J. L. Dubois, J. Gazave, G. Gregori, E. D'humières, S. Hulin, K. Ishihara, S. Kojima, E. Loyez, J. R. Marquès, A. Morace, P. Nicolaï, O. Peyrusse, A. Poyé, D. Raffestin, J. Ribolzi, M. Roth, G. Schaumann, F. Serres, V. T. Tikhonchuk, P. Vacar, and N. Woolsey, "Laser-driven platform for generation and characterization of strong quasi-static magnetic fields," New J. Phys. **17**, 083051 (2015); arXiv:1503.00247.

[21]K. F. Law, M. Bailly-Grandvaux, A. Morace, S. Sakata, K. Matsuo, S. Kojima, S. Lee, X. Vaisseau, Y. Arikawa, A. Yogo, K. Kondo, Z. Zhang, C. Bellei, J. J. Santos, S. Fujioka, and H. Azechi, "Direct measurement of kilo-tesla level magnetic field

generated with laser-driven capacitor-coil target by proton deflectometry," Appl. Phys. Lett. **108**, 091104 (2016).
[22]L. Gao, H. Ji, G. Fiksel, W. Fox, M. Evans, and N. Alfonso, "Ultrafast proton radiography of the magnetic fields generated by a laser-driven coil current," Phys. Plasmas **23**, 043106 (2016).
[23]Z. Zhang, B. Zhu, Y. Li, W. Jiang, D. Yuan, H. Wei, G. Liang, F. Wang, G. Zhao, J. Zhong, B. Han, N. Hua, B. Zhu, J. Zhu, C. Wang, Z. Fang, and J. Zhang, "Generation of strong magnetic fields with a laser-driven coil," High Power Laser Sci. Eng. **6**, e38 (2018).
[24]B. Zhu, Z. Zhang, W. Jiang, J. Wang, C. Zhu, J. Tan, Y. Zhang, Y. He, Y. Li, J. Ma, and Y. Li, "Ultrafast pulsed magnetic fields generated by a femtosecond laser," Appl. Phys. Lett. **113**, 072405 (2018).
[25]B. Zhu, Z. Zhang, W. Jiang, J. Wang, C. Zhu, J. Tan, Y. Zhang, Y. He, Y. Li, J. Ma, and Y. Li, "Effects of pulse duration on magnetic fields generated with a laser-driven coil," High Energy Density Phys. **37**, 100900 (2020).
[26]G. Liao, Y. Li, B. Zhu, Y. Li, F. Li, M. Li, X. Wang, Z. Zhang, S. He, W. Wang, F. Lu, F. Zhang, L. Yang, K. Zhou, N. Xie, W. Hong, Y. Gu, Z. Zhao, B. Zhang, and J. Zhang, "Proton radiography of magnetic fields generated with an open-ended coil driven by high power laser pulses," Matter Radiat. Extremes **1**, 187–191 (2016).
[27]O. Chubar, P. Elleaume, and J. Chavanne, "A three-dimensional magnetostatics computer code for insertion devices," J. Synchrotron Radiat. **5**, 481–484 (1998).
[28]E. U. Condon and G. H. Shortley, *The Theory of Atomic Spectra*, Cambridge University Press Vol. 209 (Cambridge University Press, 1935), Harvey B. Plotnick collection of the history of quantum mechanics, and the theory of relativity.
[29]A. Kramida, Yu. Ralchenko, J. Reader, and NIST ASD Team, NIST Atomic Spectra Database (ver. 5.8), available at https://physics.nist.gov/asd (January 31, 2016), National Institute of Standards and Technology, Gaithersburg, MD, 2020.
[30]F. Paschen and E. Back, "Normale und anomale Zeemaneffekte," Ann. Phys. **344**, 897–932 (1912).
[31]F. F. Chen, *Introduction to Plasma Physics and Controlled Fusion* (Springer, Cham, 2016).
[32]J. J. MacFarlane, I. E. Golovkin, P. R. Woodruff, D. R. Welch, B. V. Oliver, T. A. Mehlhorn, and R. B. Campbell, "Simulation of the ionization dynamics of aluminum irradiated by intense short-pulse lasers," in *Inertial Fusion Sciences and Applications 2003* (Springer, Cham, 2004), pp. 457–460.
[33]B. N. Murdin, J. Li, M. L. Pang, E. T. Bowyer, K. L. Litvinenko, S. K. Clowes, H. Engelkamp, C. R. Pidgeon, I. Galbraith, N. V. Abrosimov, H. Riemann, S. G. Pavlov, H. W. Hübers, and P. G. Murdin, "Si:P as a laboratory analogue for hydrogen on high magnetic field white dwarf stars," Nat. Commun. **4**, 1469 (2013).
[34]J. Liebert, H. C. Harris, C. C. Dahn, G. D. Schmidt, S. J. Kleinman, A. Nitta, J. Krzesiski, D. Eisenstein, J. A. Smith, P. Szkody, S. Hawley, S. F. Anderson, J. Brinkmann, M. J. Collinge, X. Fan, P. B. Hall, G. R. Knapp, D. Q. Lamb, B. Margon, D. P. Schneider, and N. Silvestri, "SDSS white dwarfs with spectra showing atomic oxygen and/or carbon lines," Astrophys. J. **126**(5), 2521 (2003).